MESHLESS ANALYSIS OF LINEAR ELASTOSTATIC PLANE PROBLEMS

M.Riyad Abdelkader*, A.Sahli, O.Rahmani

***University of Jordan**
Department of Mechanical Engineering
Faculty of Engineering & Technology
P.O Box 13258 Amman, Jordan

Faculté de Mécanique USTO
Département de Génie Mécanique
B.P 1505 El-M'Naouer Oran, ALGERIE

Abstract: This method is a "true" meshless method and does not need any "element" or "mesh" but uses a distributed set of nodes for both field interpolation and background integration. The Meshless Local Petrov-Galerkin (MLPG) method is adopted to solve plane stress/ strain solid mechanics problems. The MLPG method requires only a set of nodes both for the interpolation of the solution variables and the evaluation of various integrals appearing in the problem formulation. The MLPG formulation including the moving least squares method, the choice of the weight function, the local symmetric weak form (LSWF), and the discretization of the weak form are presented. A code based on the MLPG method is developed, and three numerical examples, namely, a cantilever beam loaded by tangential tractions at the unclamped edge, an infinite plate with a circular hole subjected to a uniform tensile force at infinity, and a hollow circular cylinder subjected to a pressure on the inner surface are demonstrated to validate the developed code.

Key-words: MLPG; Moving least squares (MLS) approximation; Weight function; local symmetric weak form.

1 Introduction

A large variety of different meshless methods have been developed in the last few years such as the Smooth Particle Hydrodynamics (SPH), the Diffuse Element Method (DEM), the Element-Free Galerkin (EFG) method, the Hp-Clouds, the Reproducing Kernel Particle Method (RKPM), the Partition of Unity Finite Element Method (PUFEM), and the Meshless Local Petrov-Galerkin method (MLPG). All meshless methods share a common feature: only nodes are required to describe the interpolation of field variables. The major difference among these methods lies in the interpolation techniques. Generally, three different interpolation techniques used in meshless methods are the kernel method, the moving least squares approximation and the partition of unity.

Although the meshless method is just becoming popular in recent years, the initial use of this method dates back to the late 1970's. Lucy [1] introduced the Smooth Particle Hydrodynamics (SPH) for simulating astrophysical phenomena. Monaghan [2] provided a theoretical aspect for the interpolation scheme of the SPH by adopting the notion of a kernel function. This kernel function allows a local representation for the trial function. Libersky and Petchek [3] applied this method to solve solid mechanics problems. Nayroles et al. [4] proposed another branch of the meshless method under the name of the Diffuse Element Method (DEM). This method is based on the moving least squares (MLS) approximation which had been developed by Lancaster and Salkauskas [5] for curve and surface fitting of random data. Belytschko et al. [6] made improvements to the DEM and developed the Element Free Galerkin (EFG) method. For example, a high-order quadrature rule based on a background mesh of cells was used and certain terms in the derivatives of the interpolants, which were omitted in the DEM, were included in the EFG method. These improvements were found to be necessary for achieving good accuracy and convergence.

Liu et al. [7] introduced a correction function in the kernel of the integral transformation in the SPH to impose reproducing conditions (i.e., consistency requirements). Adding this correction function in the kernel enhances the accuracy of the solution when compared with the SPH. This method using integral transformation with a corrected kernel function is called the Reproducing Kernel Particle Method (RKPM). Belytschko et al. [8] have shown that the discrete form of the convolution integral yields approximants which are identical to those in the MLS approximation.

Duarte and Oden [9], and Melenk and Babuska [10] proposed the Hp-Clouds method and the Partition of Unity Finite Element Method (PUFEM), respectively. Both methods employ a partition of unity to construct the meshless approximation. They recognized that the method based on

the moving least squares is a specific case of the partition of unity. The Hp-Clouds and the PUFEM allow for an extrinsic basis to enhance the solution.

Similarities in some of the above meshless methods have been summarized by Belytschko et al.[8]. However, the above-mentioned meshless methods use background cells or shadow elements to integrate a global Galerkin weak formulation. The requirement of background cells for integration implies that the method is not "truly meshless".

The meshless methods are not computationally as efficient as finite element methods. It is desirable to use the meshless model only in those domains where their greater versatility is needed and the finite element model for the rest of the domain and on the boundary where the essential boundary conditions can be exactly satisfied. Liu and Gu [11] coupled the MLPG method with either the finite element or the boundary element method to enhance the efficiency of the MLPG method.

2 MLPG weak formulation

Consider the following two-dimensional elasto-statics problem on the domain Ω bounded by the boundary Γ :

$$\sigma_{ij,j} + b_i = 0, \quad in \quad \Omega, \tag{1}$$

where σ_{ij} is the stress tensor, bi is the body force. The boundary conditions are given as follows:

$$\begin{aligned} u_i &= \overline{u}_i \quad on \quad \Gamma_u, \\ t_i &= \sigma_{ij} n_j = \overline{t}_i \quad on \quad \Gamma_t, \end{aligned} \tag{2}$$

where $\overline{u}_i$ and $\overline{t}_i$ are the prescribed displacements and tractions, respectively, on the boundary Γ_u and the boundary, Γ_t and n_i is the unit outward normal to the boundary Γ, Γ_u and $\Gamma_t$are complementary subsets of Γ.

Unlike the Element Free Galerkin (EFG) method which is based on the global Galerkin formulation, the present local Petrov-Galerkin formulation is constructed over a local sub domain Ω_s which is located inside the global domain Ω. This local sub-domain Ω_s is taken to be either a circle or a part of a circle in a 2-D problem [12] [13].

A generalized local weak form of Eq. (1) and Eq. (2) over a local sub-domain Ω_s can be written as follows:

$$\int_{\Omega_s} (\sigma_{ij,j} + b_i) v_i \, d\Omega - \int_{\Gamma_{su}} \alpha (u_i - \overline{u}_i) v_i \, d\Gamma = 0, \tag{3}$$

where u_i and v_i are the trial and the test functions, respectively, and Γ_{su} is the part of the boundary $\partial\Omega_s$ over which essential boundary conditions are specified. In general, $\partial\Omega_s = \Gamma_s \cup L_s$ with Γ_s being the part of the local boundary located on the global boundary and L_s being the other part of the local boundary over which no boundary condition is specified, i.e., $\Gamma_s = \partial\Omega_s \cap \Gamma$ and $\Gamma_s = \partial\Omega_s - L_s$ (see Fig. 1). In Eq. (3), α is a penalty parameter ($\alpha >>$ Young's modulus/Length) which is used to impose the essential boundary conditions. Also, the dimensions of α are such that the two terms in Eq. (3) have the same units. α could be a function of $\boldsymbol{x}$ but is usually taken to be a constant. Henceforth, we also take α to be a constant [14].

Using $\sigma_{ij,j} v_i = (\sigma_{ij} v_i)_{,j} - \sigma_{ij} v_{i,j}$ and the divergence theorem in Eq. (3) lead to

$$\int_{\partial\Omega_s} \sigma_{ij} n_j v_i \, d\Gamma - \int_{\Omega_s} (\sigma_{ij} v_{i,j} - b_i v_i) \, d\Omega - \alpha \int_{\Gamma_{su}} (u_i - \overline{u}_i) v_i \, d\Gamma = 0, \tag{4}$$

where ni is a unit outward normal to the boundary $\partial\Omega_s$.

It should be mentioned that Eq. (4) holds regardless of the size and the shape of Ω_s provided that Ω_s is smooth enough for the divergence theorem to apply. So, the shape of a sub-domain Ω_s can be taken to be a circle in 2-D problems without loosing generality.

Applying the natural boundary condition, $t_i = \sigma_{ij} n_j = \overline{t}_i$ on Γ_{st} where $\Gamma_{st} = \partial\Omega_s \cap \Gamma_t$, we get

$$\begin{aligned} &\int_{L_s} t_i v_i \, d\Gamma + \int_{\Gamma_{su}} t_i v_i \, d\Gamma + \int_{\Gamma_{st}} \overline{t}_i v_i \, d\Gamma - \\ &\int_{\Omega_s} (\sigma_{ij} v_{i,j} - b_i v_i) \, d\Omega - \alpha \int_{\Gamma_{su}} (u_i - \overline{u}_i) v_i \, d\Gamma = 0, \end{aligned} \tag{5}$$

In order to simplify equation (5), the test functions vi are chosen such that they vanish on Ls. This can be accomplished by using the weight function wi in the moving least squares (MLS) approximation as also the test function vi, but the radius ri of the support of the weight function is replaced by the radius ro of the local domain Ω_s. Using these test functions and rearranging Eq. (5), we obtain the following local symmetric weak form (LSWF):

$$\begin{aligned} &\int_{\Omega_s} \sigma_{ij} v_{i,j} \, d\Omega + \alpha \int_{\Gamma_{su}} u_i v_i \, d\Gamma - \int_{\Gamma_{su}} t_i v_i \, d\Gamma \\ &= \int_{\Gamma_{st}} \overline{t}_i v_i \, d\Gamma + \alpha \int_{\Gamma_{su}} \overline{u}_i v_i \, d\Gamma + \int_{\Omega_s} b_i v_i \, d\Omega \end{aligned} \tag{6}$$

For 2-D problems, two independent sets of test functions should be applied in Eq. (6), which gives

$$\begin{aligned} &\int_{\Omega_s} \sigma_{ij} v_{ki,j} \, d\Omega + \alpha \int_{\Gamma_{su}} u_i v_{ki} \, d\Gamma - \int_{\Gamma_{su}} t_i v_{ki} \, d\Gamma \\ &= \int_{\Gamma_{st}} \overline{t}_i v_{ki} \, d\Gamma + \alpha \int_{\Gamma_{su}} \overline{u}_i v_{ki} \, d\Gamma + \int_{\Omega_s} b_i v_{ki} \, d\Omega \end{aligned} \tag{7}$$

where vki is the ith component of the kth test function. For simplicity, Eq. (7) can be written in matrix form as:

$$\int_{\Omega_s} \varepsilon_v \sigma \, d\Omega + \alpha \int_{\Gamma_{su}} \mathrm{vu} \, d\Gamma - \int_{\Gamma_{su}} \mathrm{vt} \, d\Gamma = \int_{\Gamma_{st}} \mathrm{v}\bar{t} \, d\Gamma + \alpha \int_{\Gamma_{su}} \mathrm{v}\bar{u} \, d\Gamma + \int_{\Omega_s} \mathrm{vb} \, d\Omega \tag{8}$$

where ε_v denotes the strain matrix derived from the test functions, and σ is the stress vector derived from the trial functions. That is,

$$\sigma = \begin{Bmatrix} \sigma_{11} \\ \sigma_{22} \\ \sigma_{12} \end{Bmatrix}, \qquad \varepsilon_v = \begin{bmatrix} \varepsilon_{11}^1 & \varepsilon_{22}^1 & \gamma_{12}^1 \\ \varepsilon_{11}^2 & \varepsilon_{22}^2 & \gamma_{12}^2 \end{bmatrix}, \tag{9}$$

where the superscript i denotes the ith test function. Functions v, u, t, and b are defined as follows:

$$\mathrm{v} = \begin{bmatrix} v_{11} & v_{12} \\ v_{21} & v_{22} \end{bmatrix}, \qquad \mathrm{u} = \begin{Bmatrix} u_1 \\ u_2 \end{Bmatrix}, \qquad \mathrm{t} = \begin{Bmatrix} t_1 \\ t_2 \end{Bmatrix}, \qquad \mathrm{b} = \begin{Bmatrix} b_1 \\ b_2 \end{Bmatrix}. \tag{10}$$

The two sets of test functions **v** in Eq. (10) should be linearly independent. The simplest choice for **v** is

$v_{ij} = v \, \delta_{ij}$ or $\mathbf{v} = v \, \mathbf{I}$,

Where δ_{ij} is the Kronecker delta and **I** is the identity matrix.

As long as the union of all local sub-domains covers the global domain, the equilibrium equations (1) and the boundary conditions (2) will be satisfied in the global domain Ω and on its boundary Γ respectively.

3 Discretization of the weak form

In the MLPG method, the field variable $u(x)$ is approximated by the moving least squares (MLS) technique. This approximation is based on three components: a weight function of compact support associated with each node, polynomial basis functions, and a set of coefficients that depend on the position $\boldsymbol{x}$ of the point.

First, we consider a sub-domain Ω_x called the domain of definition of the MLS approximation for the trial function at the point x, which is located in the problem domain Ω The unknown trial approximant $u^h(x)$ of the function $u(x)$ is defined by

$$u^h(x) = p^T(x) \, a(x), \qquad \forall x \in \Omega_x, \tag{11}$$

where $p^T(x) = [\, p_1(x), \, p_2(x), .., \, p_m(x)]$ is a vector of the complete monomial basis of order m, and $a(x)$ is a vector containing unknown coefficients $a_j(x), \; j = 1,2,...,m$.

The coefficient vector $a(x)$ is given by the linear relation:

$$A(x) \, a(x) = B(x) \, \hat{u}, \tag{12}$$

where

$$\begin{aligned} A(x) &= \sum_1^n w_i(x) \, p(x_i) \, p^T(x_i) \\ B(x) &= \left[w_1(x) \, p(x_1), w_2(x) \, p(x_2), ..., w_n(x) \, p(x_n) \right] \\ \hat{u}^T &= \left[\hat{u}_1, \hat{u}_2, ..., \hat{u}_n \right] \end{aligned} \tag{13}$$

where $w_i(x)$ is the weight function associated with the node i with $w_i(x) > 0$ for all x in the support of $w_i(x)$, x_i denotes the value of x at node i, n is the number of nodes in Ω_x for which the weight functions $w_i(\boldsymbol{x}) > 0$, and $\hat{u}_i$ is the fictitious nodal value and need not equal $u^h(x_i)$.

As can be seen from Eq. (12), the unknown coefficients $a(x)$ can be obtained only if $A(x)$ defined by Eq. (13) is non-singular. So, a necessary condition for a well-defined MLS approximation is that at least m weight functions are non-zero (i.e. $n \geq m$) for each sample point $x \in \Omega$.

Substituting for $a(x)$ into Eq. (11) gives the following relation for nodal interpolation

$$u^h(x) = \sum_1^n \phi_i(x) \hat{u}_i, \quad u^h(x_i) \equiv u_i \neq \hat{u}_i, \quad x \in \Omega_x, \tag{14}$$

where

$$\phi_i(x) = \sum_{j=1}^m p_j(x) \left[A^{-1}(x) \, B(x) \right]_{ji} \tag{15}$$

$\varphi_i(x)$ is usually called the shape function of the MLS approximation corresponding to node i.

Substituting the MLS approximation (14) into Eq. (8) and summing over all nodes leads to the following discretized system of linear equations:

$$\begin{aligned} &\sum_{j=1}^n \int_{\Omega_s} \varepsilon_v(x,x_i) D B_j \, \hat{\mathrm{u}}_j \, d\Omega + \alpha \sum_{j=1}^n \int_{\Gamma_{su}} \mathrm{v}(x,x_i) S \phi_j \, \hat{\mathrm{u}}_j \, d\Gamma \\ &- \sum_{j=1}^n \int_{\Gamma_{su}} \mathrm{v}(x,x_i) N D S B_j \, \hat{\mathrm{u}}_j \, d\Gamma = \\ &\int_{\Gamma_{st}} \mathrm{v}(x,x_i) \bar{t} \, d\Gamma + \alpha \int_{\Gamma_{su}} \mathrm{v}(x,x_i) S \bar{\mathrm{u}} \, d\Gamma + \int_{\Omega_s} \mathrm{v}(x,x_i) \mathrm{b} \, d\Omega \end{aligned} \tag{16}$$

where $\mathrm{v}(x, x_i)$ is the value at x of the test function, corresponding to node i, and

$$N = \begin{bmatrix} n_1 & 0 & n_2 \\ 0 & n_2 & n_1 \end{bmatrix}$$

$$B_j = \begin{bmatrix} \phi_{j,1} & 0 \\ 0 & \phi_{j,2} \\ \phi_{j,2} & \phi_{j,1} \end{bmatrix}$$

$$D = \frac{\overline{E}}{1-\overline{\nu}^2} \begin{bmatrix} 1 & \overline{\nu} & 0 \\ \overline{\nu} & 1 & 0 \\ 0 & 0 & (1-\overline{\nu})/2 \end{bmatrix} \tag{17}$$

We note that

$$\overline{E} = \begin{cases} E \\ E/(1-\nu^2) \end{cases}, \quad \overline{\nu} = \begin{cases} \nu & \text{for plane stress,} \\ \nu/(1-\nu^2) & \text{for plane strain,} \end{cases} \tag{18}$$

and

$$S = \begin{bmatrix} S_1 & 0 \\ 0 & S_2 \end{bmatrix}, \quad S_i = \begin{cases} 1 & \text{if } u_i \text{ is prescribed on } \Gamma_u, \\ 0, & \text{if } u_i \text{ is not prescribed on } \Gamma_u, \end{cases} \tag{19}$$

Eq. (16) can be simplified into the following system of linear algebraic equations in $\hat{u}_j$.

$$\sum_{j=1}^{N} K_{ij}\, \hat{u}_j = f_i, \qquad i = 1,2,\ldots,N, \tag{20}$$

where N is the total number of nodes. The so-called "stiffness" matrix K and the "load" vector f are defined by

$$K_{ij} = \int_{\Omega_s} \varepsilon_v(x,x_i)\, D\, B_j\, d\Omega + \alpha \int_{\Gamma_{su}} v(x,x_i)\, S\, \phi_j - \int_{\Gamma_{su}} v(x,x_i)\, N\, D\, B_j\, S\, d\Gamma, \tag{21}$$

and

$$f_i = \int_{\Gamma_{st}} v(x,x_i)\, \bar{t}\, d\Gamma + \alpha \int_{\Gamma_{su}} v(x,x_i)\, S\, \bar{u}\, d\Gamma + \int_{\Omega_s} v(x,x_i)\, b\, d\Omega \tag{22}$$

4 Validation of the Code

Based on the MLPG method described above, we have developed a computer code to solve plane stress/strain elastostatics problems. This code is validated by solving the following three elasticity problems each of which has an analytical solution (exact solution taken from [14]).

.

- The first problem studied is a cantilever beam (Fig. 1) deformed by applying a tangential traction on the unclamped end. We impose the following boundary conditions at the bounding surfaces of the beam.

Displacements are specified at nodes on the left edge, and tractions are prescribed at the remaining three surfaces of the beam. This is solved as a plane stress problem. In a consistent set of units, we take $P = 1$ (is the resultant of the tangential tractions applied at the unclamped edge), E = 1000MPa, D = 1m, L = 8m, ν = 0.25 and the penalty parameter $\alpha = 10^8$. A regular nodal mesh of 72 nodes with 18 nodes along the x^1 direction and 4 nodes along the x^2 direction is used. The radius r_o of the local sub-domain is taken to be the distance between two neighbouring nodes in x^2 direction. In the computation, 8x 8 Gauss points are used in each local sub-domain Ω_s and 8 Gauss points are used along each section of Γ_s.

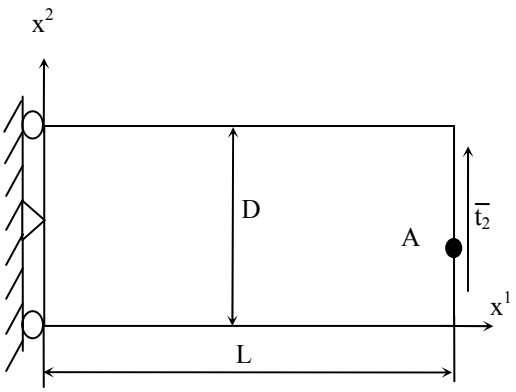

Figure 1: The cantilever beam

Figures 2, 3 and 4 show, respectively, the variations of the horizontal displacement u_1, the vertical displacement u_2, and the longitudinal stress σ_{11} vs. x^1 on the top face. It is clear that these agree very well with the analytical solution. Figures 5 and 6 illustrate the through-the-thickness variation of the normal stress σ_{11} and the shear stress σ_{12} at $x^1 = L/2 = 4m$. Both stress components are almost the same as those in the exact solution.

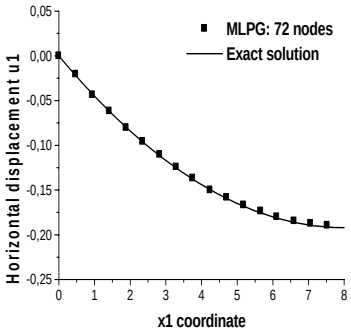

Figure 2: Horizontal displacement u_1 vs. x^1 on the top face

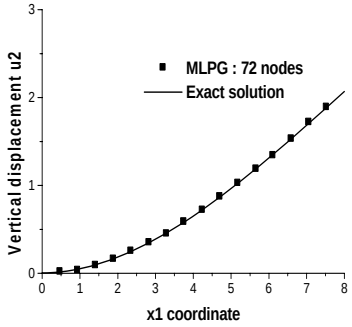

Figure 3: Vertical displacement u_2 vs. x^1 on the top face

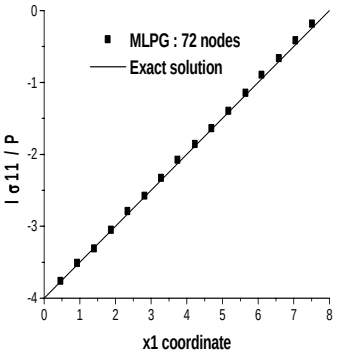

Figure 4: σ_{11} vs. x^1 on the top face

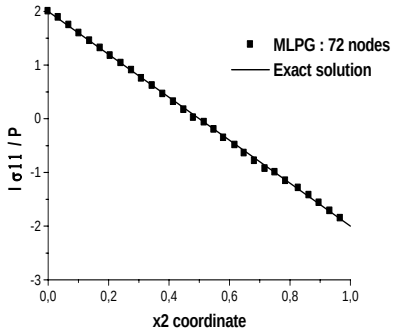

Figure 5: Through-the-thickness distribution of σ_{11} on the plane $x^1 = 4$m

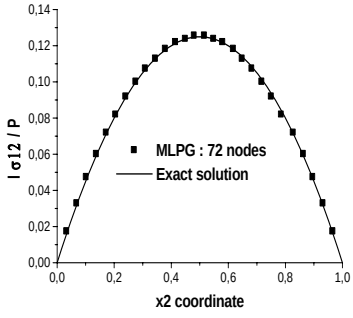

Figure 6: Through-the-thickness distribution of $\sigma_{1\ 2}$ on the plane $x^1 =$

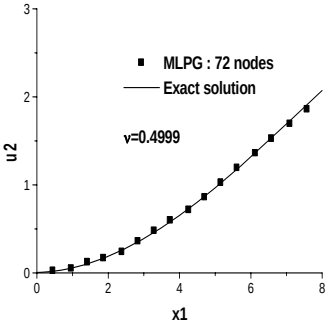

*Figure 7*a*:* Vertical displacement u_2 vs. x^1 on the top face

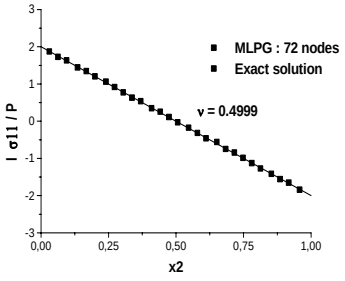

*Figure 7*b*:* σ_{11} vs. x^1 on the top face.

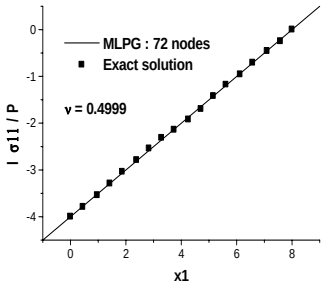

Figure 7c: σ_{11} vs. x^2 at $x^1 = 4$m

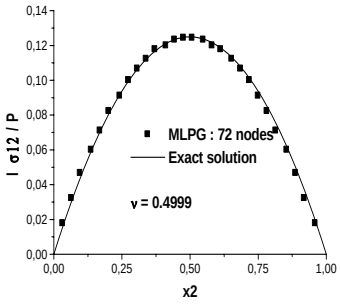

Figure 7d: σ_{12} vs. x^2 at $x^1 = 4$m

We now examine if the MLPG method gives good results for nearly incompressible materials by taking ν=0.4999. As can be seen in Figs. 7a-7d, the numerical solution matches well with the analytical solution. Figures 7c and 7d show respectively the normal stress σ_{11} and the shear stress σ_{12} at $x^1 = L/2 = 4m$ along the thickness direction. It is found that

the MLPG method does not exhibit the locking phenomenon seen in the Finite Element Method.
The deflection at point A (shown in Fig. 3) computed by the FE and the MLPG methods are compared in the following table; the FE solution is taken from [6]. A plane strain state rather than a plane stress state of deformation is assumed to prevail in the beam.

u_2^{num} / u_2^{exact} at point A (plane strain case)		
Method	ν = 0.25	ν = 0.4999
FEM : Q4	0.824	0.027
MLPG : linear	1.000	1.007
MLPG : quadratic	1.000	1.000

Table 1.1

It is obvious that the FEM using the 4-node quadrilateral element (Q4) performs poorly especially when ν = 0.4999 while the MLPG method works well. A similar trend was observed by [15] in their analysis of the problem.

- Consider an infinite plate with a circular hole and subjected to a unit normal traction at infinity in the x^1 direction. Due to the symmetry of the problem about the horizontal and the vertical centroidal axes, only the upper right quadrant of the plate, shown in Fig. 8, is considered. This quadrant is modelled as a square plate with the length of a side equal to *4*a. Boundary conditions resulting from the symmetry of the problem are imposed on the left and the bottom edges, and the boundary of the hole is traction free.

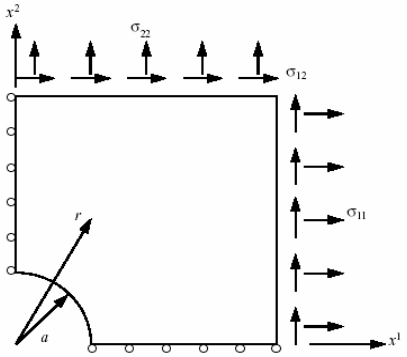

Figure8: The analysis domain for a plate with a circular hole.

Traction boundary conditions are imposed on the right *(*x^1 = *4*a) and the top *(*x^2 = *4*a) edges. A plane stress state of deformation is assumed to prevail in the plate. In a consistent set of units, we take *E = 1000MPa, v = 0.25*, and *a = 1m* in this computation. Two different nodal meshes with 49 (7x7: 7 nodes in the *r* direction, 7 nodes in the θ direction) and 81 (9x9) nodes are considered. 9x9 Gauss points are used in each local sub-domain Ω_s and 9 Gauss points are used on each section of Γ_s for numerical integration.
The stress σ_{11} at x^1 =0 using a linear basis is compared with the analytical solution in Fig.9. It can be seen that the stress σ_{11} is very well approximated when the number of nodes is increased to 81.

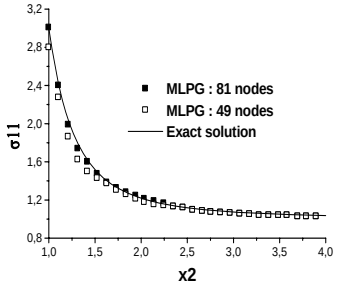

Figure 9: σ_{11} vs. x^2 at $x^1 = 0$.

- Consider a hollow cylinder subjected to tractions as shown in Fig. 10. Due to the symmetries about the horizontal and the vertical centroidal axes, only a quarter of the cylinder is modelled with 840 nodes. A plane strain state of deformation is assumed to prevail in the plate. In a consistent set of units, we take *E = 1000MPa, v = 0.25, a = 5m, b = 10m,* p_b *= 0 Pa,* p_a *= 1Pa. Symmetry* boundary conditions are applied on the left and the bottom edges.

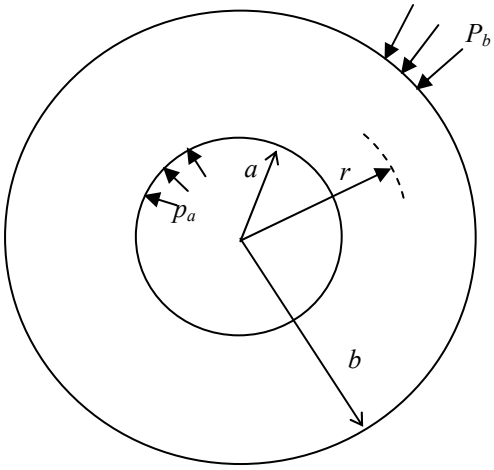

Figure 10 : A hollow circular cylinder with pressure applied on the inner and outer surfaces.

Weight function and the number of quadrature points used are the same as in the previous problem of an infinite plate with a circular hole.
Figures 11 a-c show that the deformation and the stress fields obtained by the MLPG method match well with the analytical solution. It is noted that the MLPG method satisfies the traction boundary conditions (p_a = *-1Pa* at r = 5m and p_b = *0Pa* at *r = 10m*) almost exactly. Fig. 11d verifies that $\sigma_{rr} + \sigma_{\theta\theta}$ is constant throughout the wall of the cylinder.

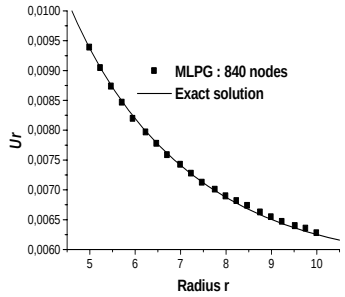

Figure 11(a)

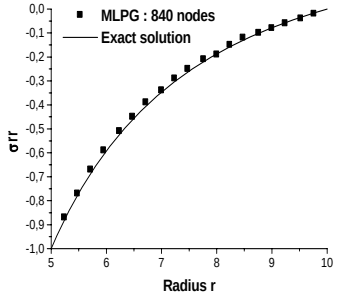

Figure 11(b)

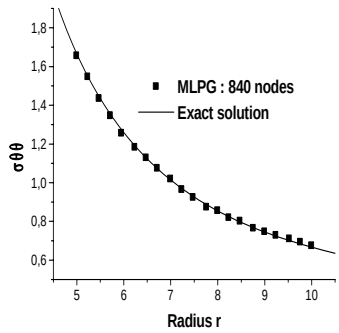

Figure 11(c)

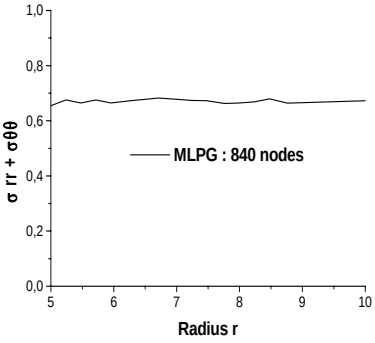

Figure 11(d)

Figure 11: (a) u_r vs. r
(b) σ_{rr} vs. r
(c) $\sigma_{\theta\theta}$ vs. r
(d) $\sigma_{rr} + \sigma_{\theta\theta}$ vs. r

5 - Conclusion

The MLPG method proposed in this paper is an effective numerical technique for the solution of the linear elastostatic plane problems.

A system of linear algebraic equations has been deduced starting from the moving least squares approximation and the weak formulation. The approximation of the field variable in the MLPG method is based on three components: a weight function of compact support associated with each node, polynomial basis functions, and a set of coefficients that depend on the position of the point. The implementation of a numerical code has thus been completed using the Gaussian weight function.

The computational examples presented above have shown that the current MLPG method could be applied efficiently to the analysis of the plane strain/stress solid mechanics problems. Comparison of the numerical results obtained by the present MLPG method, with those calculated from the analytical solution, shows that the MLPG technique achieves a satisfaction degree of accuracy.

REFERENCES

[1] Lucy L. B., A numerical approach to the testing of the fission hypothesis. *The Astronomical Journal* 82(12), (1977) 1013-1024.

[2] Monaghan J. J., Why particle methods work. *SIAM Journal of Scientific and Statistical Computing* 3(4), (1982) 422-434.

[3] Libersky L. D. and Petschek A. G., Smoothed particle hydrodynamics with strength of materials. In H. Trease, J. Fritts, and W. Crowley (Eds.), *The Next Free Lagrange Conference*, (1991) 248-257.

[4] Nayroles B., Touzot G. and Villon P., Generalizing the finite element method: diffuse approximation and diffuse elements. *Computational Mechanics* 10, (1992) 307-318.

[5] Lancaster P. and Salkauskas K., Surfaces generated by moving least squares methods. *Mathematics of Computation 37*, (1981) 141-158.

[6] Belytschko T., Lu Y. Y. and Gu L., Element-free Galerkin methods. *International Journal for Numerical Methods in Engineering*, 37, (1994) 229-256.

[7] Liu W. K., Jun S. and Zhang Y. F., Reproducing kernel particle methods. *International Journal for Numerical Methods in Engineering* 20, (1995) 1081-1106.

[8] Belytschko T., Krongauz Y, Organ D. J., Fleming M. and Krysl P., Meshless methods: An overview and recent developments. *Computer Methods in Applied Mechanics and Engineering*, (1996) 139, 3-47.

[9] Duarte C. A. and Oden J. T., H-*p* clouds . an *hp* meshless method. *Numerical Methods for Partial Differential Equations*, (1996) 1-34.

[10] Melenk J. M. and Babuska I., The partition of unity finite element method: Basic theory and applications. *Computer Methods in Applied Mechanics and Engineering,* (1996).

[11] Liu G. R. and Gu Y. T., Meshless Local Petrov-Galerkin (MLPG) method in combination with finite element and boundary element approaches. *Computational Mechanics*, 26(6), (2000) 536-546.

[12] Atluri, S. N. and Zhu, T., A new Meshless Local Petrov-Galerkin (MLPG) approach in computational mechanics. *Computational Mechanics*, vol. 22, (1998) pp. 117-127.
[13] Lin, H. and Atluri, S. N., Meshless local Petrov-Galerkin (MLPG) method for convection-diffusion problems. *Computer Modelling in Engineering and Sciences*, vol. 1, (2000) pp.45-60.
[14] Atluri, S. N., Kim, H. G. and Cho J. Y., A critical assessment of the truly meshless local Petrov-Galerkin (MLPG) and local boundary integral equation (LBIE) methods. *Computational Mechanics*, vol 24, (1999) pp. 348-372.
[15] Timoshenko S. P. and Goodier J. N., *Theory of Elasticity* (Third Ed.). New York: McGraw Hill, 1970.